International Journal of GEOMATE, June, 2022, Vol.22, Issue 94, pp.13-20
ISSN: 2186-2982 (P), 2186-2990 (O), Japan, DOI: https://doi.org/10.21660/2022.94.97
Geotechnique, Construction Materials and Environment

SLOPE DEFORMATION MONITORING USING WIRELESS SENSOR NETWORK AND EVALUATION OF MECHANICAL STABILITY BY FDM SIMULATION

*Satoshi Sugimoto[1] and Yoichi Ishizuka[1]

[1]Faculty of Engineering, Nagasaki University, Japan

*Corresponding Author, Received: 21 Feb. 2022, Revised: 08 March 2022, Accepted: 02 April 2022

ABSTRACT: In recent years, torrential rains have occurred frequently owing to abnormal weather and the rainy season, thereby resulting in numerous slope failures. When rainfall occurs, the infiltration of rainwater and the inflow of groundwater from upstream may reduce the shear resistance in the slope, and the infiltration water pressure may result in slope failure. In addition, the change in groundwater on natural slopes is significant, and the amount of groundwater inflow from upstream increases, which may result in slope failure. The purpose of this study is to reproduce and stabilize the increase in groundwater level on the target slope via numerical analysis and to consider the effect of hydraulic conductivity on groundwater level increase and the safety factor. In addition, we propose a method for observing the penetration of groundwater due to rainfall and the change in groundwater depth using a wireless sensor network for sedimentation grounds. Furthermore, we clarify the progress of slope deformation and the correlations between rainfall, groundwater depth fluctuation, and slope deformation.

Keywords: Wireless sensor network, Monitoring, Slope, FDM

1. INTRODUCTION

In recent years, cost constraints affecting the local administration in Japan have necessitated the unmanned management of local social infrastructure facilities. Although the infrastructure in Japan has been further developed recently, many slope failures and landslide accidents caused by earthquakes and heavy rains still occur in various regions. Hence, it may be effective to constantly monitor the indicators of disaster before it occurs in the predicted disaster area and to implement countermeasures such as prioritizing high-risk areas for construction. However, most monitoring systems used currently are wired with information collection systems, which are difficult to install in undeveloped areas, such as slopes. In addition, high-precision and expensive sensors are often used for measurement, which limits the number of measurement points owing to the cost of the system and difficulty of installation. In addition, the difficulty in securing a power source to operate the system over a long period is a major obstacle that hinders monitoring in undeveloped areas, such as slopes. Consequently, the limited amount of measurement data acquired and the localization of measurement locations hinder the effective determination of the priority of proactive measures, as described earlier.

In this study, slope deformation and changes in groundwater depth due to rainfall were observed using a wireless sensor network developed in previous studies [1]–[3] on an artificially reclaimed slope in Sasebo City, Nagasaki Prefecture, Japan. The purpose of this study is to quantitatively clarify the progression of slope deformation through continuous data acquisition and analysis and to clarify the correlation between rainfall, changes in groundwater depth, and the amount of ground deformation.

2. MEASUREMENT BY REMOTE MONITORING SYSTEM

2.1 Outline of Target Slope

The target slope shown in Fig. 1 is a slope from a former stable industrial waste disposal site located in Sasebo City; it comprises sediment-dominated industrial waste layers, talus deposit layers, and bedrock, in the order from near the ground surface.

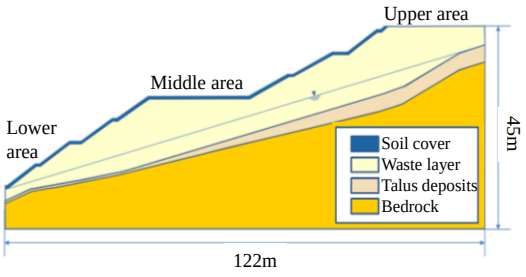

Fig. 1 Cross-section of slope.

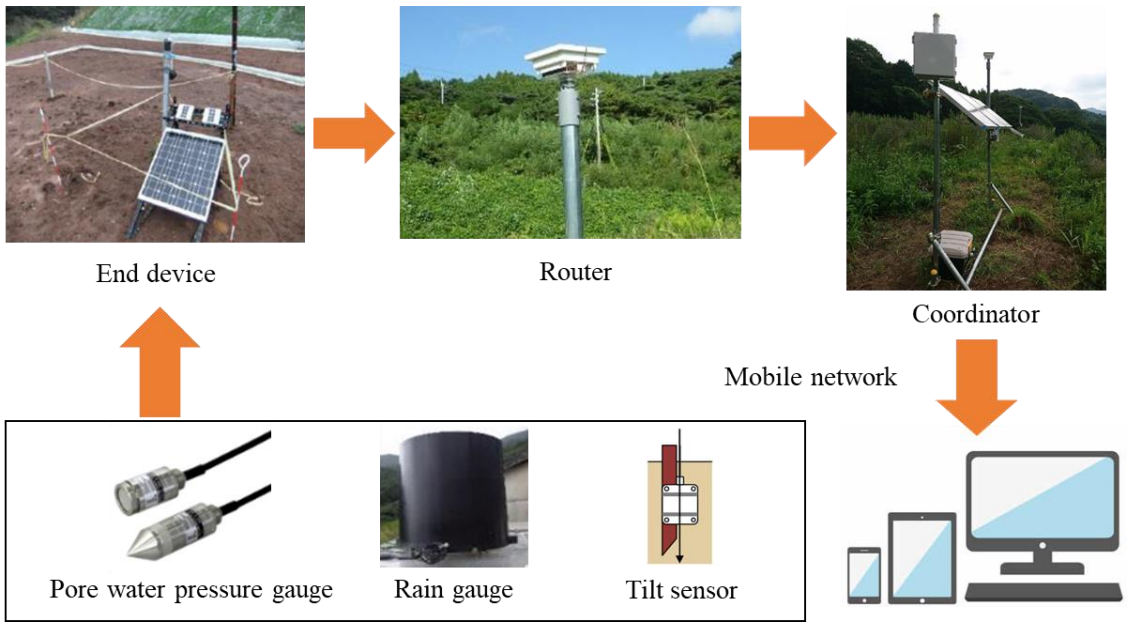

Fig. 2 Remote monitoring system.

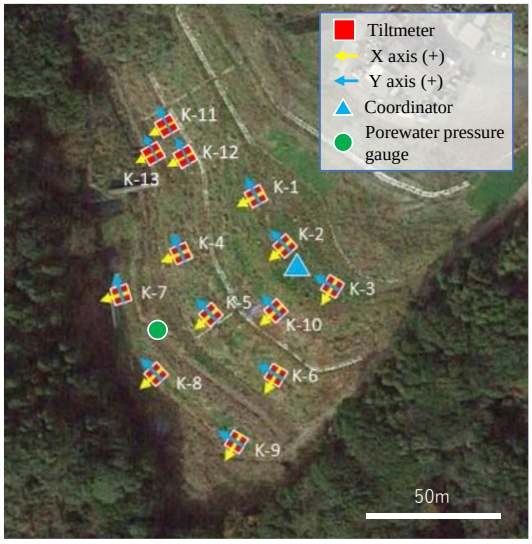

Fig. 3 Layout of installed instruments.

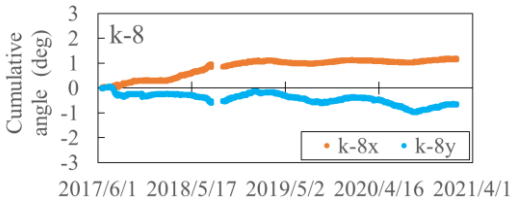

Fig. 4 Change in cumulative angle at k-8.

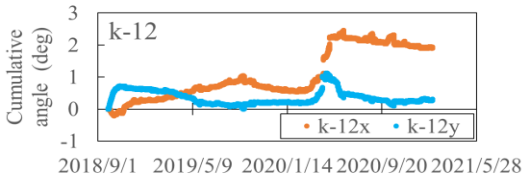

Fig. 5 Change in cumulative angle at k-12.

Heavy rains in 2013 caused deformation from the middle to the lower section of the slope. Additionally, a large-scale crack occurred near the middle section. Consequently, the slope was gently graded by cutting back the soil and intercepted by covering the surface layer with 0.5 m of soil. The current slope profile had a maximum slope gradient of approximately 35° and a height of approximately 40 m.

2.2 Overview of Monitoring System

Figure 2 shows the configuration of the remote-monitoring system developed in this study. The sensors installed on the site were connected to the communication module. The periodically recorded data were transferred from the end device to the coordinator via routers. The communication standard was Zigbee, and each device was operated with a self-supporting power supply using solar panels and lead batteries. Figure 3 shows the various monitoring instruments used and their installation locations. The mechanism of this monitoring system is as follows [4], [5]: (1) Observation data are acquired using observation devices such as a water level meter, rain gauges, and tiltmeters; (2) data are obtained using routers and a coordinator in the field through a wireless sensor network (hereinafter referred to as WSN); (3) data are transmitted to the server through a mobile communication network. Monitoring can be performed remotely, which ensures the safety of the

target slope and allows the current status to be analyzed in real-time by analyzing the sensing data. The water level meter was measured at a depth of approximately 10 m from the ground surface. The water depth can be measured at a minimum depth of 0.01 m and a maximum depth of approximately 20 m. In addition, tiltmeters for detecting slope deformation were installed 0.5 m below the ground surface at 13 locations (k-1–k-13) on the target slope. The measurement range of the tiltmeter was -30° to +30°, with a resolution of 0.02°.

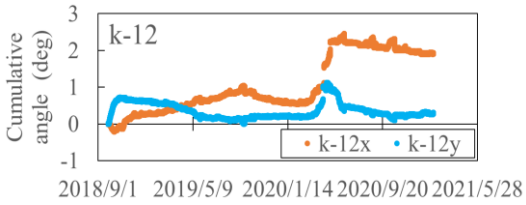

Fig. 4 Change in cumulative angle at k-8.

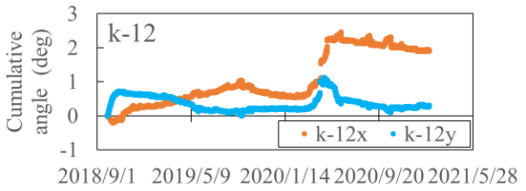

Fig. 5 Change in cumulative angle at k-12.

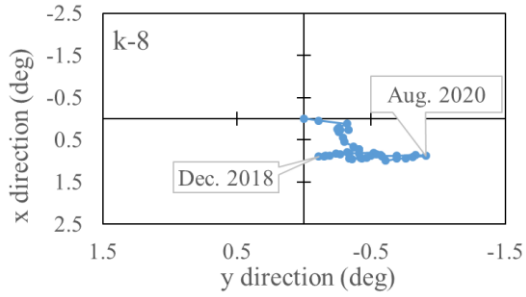

Fig. 6 Trajectory of cumulative angle at k-8.

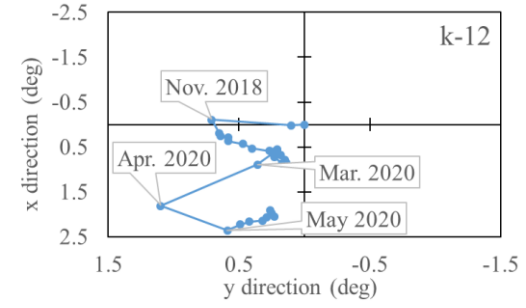

Fig. 7 Trajectory of cumulative angle at k-12.

2.3 Monitoring of Slope Surface Deformation via WSN

Based on the data from June 13, 2017, to January 31, 2021, the results at k-8 and k-12 shown in Fig. 3, which indicate a significant amount of deformation, were analyzed. Figures 4 and 5 show the cumulative angle at k-8 and k-12. Figures 6 and 7 show the cumulative angle for each month for both cases. In the case of k-12, a significant amount of deformation was observed in 2018 and 2020; it increased over the years, indicating that the deformation in the direction perpendicular to the slope was significant. The cumulative amount of deformation is represented by two-dimensional vectors for k-1 to k-13, and a visualization of the slope movement is shown in Fig. 8. The relative size of the deformation can be confirmed from this figure. The downward deformation of the slope was assumed to be associated with the mid-slope deformation. Meanwhile, the stationary lower section of the slope might be due to the parallel movement of the slope while the lower section is moving. The significant amount of deformation in k-11 and k-12 might be due to their proximity to the slope, where the failure was in progress. These results indicate that the local deformation trend of the slope can be captured in a plane.

2.4 Variation in Groundwater Depth with Rainfall

The relationship between rainfall and groundwater depth was analyzed using data from 2017 to 2020 obtained from a water level meter installed at the lower section of the slope, as shown in Fig. 3. Figure 9 shows the relationship between

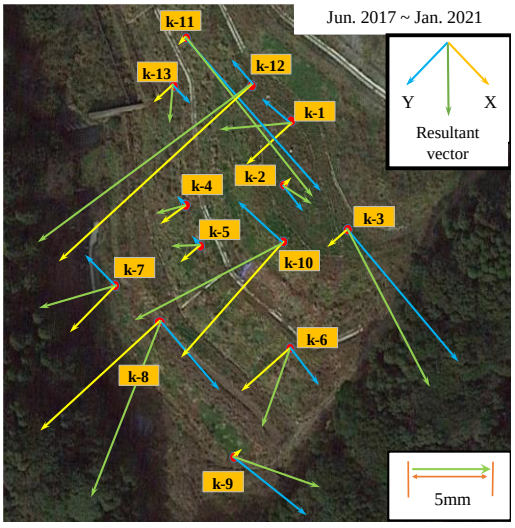

Fig. 8 Deformation vector estimated from measurement data.

rainfall and groundwater depth in 2020. Each color band in this figure indicates the period during which the increase and decrease in groundwater depth due to one rainfall event were confirmed. Figure 10 shows the relationship between rainfall and groundwater depth for the period from 2017 to 2020. The groundwater depth did not decrease annually; however, it can be assumed that it decreased in general during the period from 2017 to 2020. This may indicate an increase in the permeability of the layer where groundwater flows. Furthermore, some of the rainfall might not have infiltrated the ground but flowed out to the surface. The relationship between the rainfall coefficient Cr [6] and groundwater depth from the ground surface before rainfall is shown in Fig. 11. Cr, which is a parameter defined by Sugiyama et al., is obtained by dividing the amount of rainfall in a certain period by the amount of change in groundwater depth. Figure 11 shows the relationship between Cr and the groundwater depth before rainfall. The rainfall coefficient, Cr, is the ratio of the amount of rainfall to the increase in groundwater depth after rainfall. In the descending curve, the higher the groundwater depth from the ground surface before rainfall, the less was the increase in the groundwater depth. In the ascending curve, the increase in the groundwater depth was insignificant, despite the considerable amount of rainfall. This may be because rainfall occurred before the water depth was reduced to a steady state in response to the preceding rainfall, which may have affected the change in the rising water depth. It is expected that the correlation between rainfall and groundwater depth changes can be clarified by accumulating more data.

2.5 Relationship Between Groundwater Depth Change and Slope Deformation

The relationship between the groundwater depth and the amount of slope deformation is presented in Fig. 12, which shows the cumulative frequency of the water level increase and the inclination angles of the x-and y-axes from June to August in the abovementioned period. The cumulative frequency of the water level increase (m · h) is the frequency of the water level increase obtained by accumulating the groundwater depth from the basement rock for a certain period. The results show that the x-axis deformation was significant in 2018 in the direction perpendicular to the slope, whereas the y-axis deformation was significant in 2020. This indicates that the direction of easy movement varied by year. In addition, it was confirmed that the amount of deformation was excessive even when the cumulative frequency of the water level increase

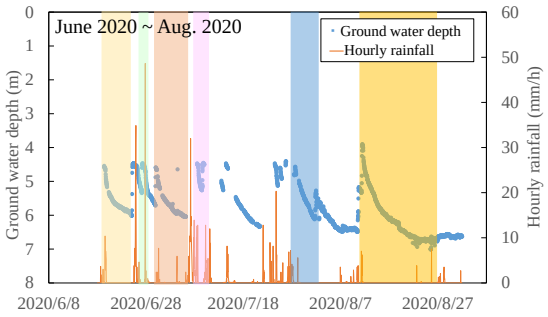

Fig. 9 Relationship between groundwater depth and rainfall.

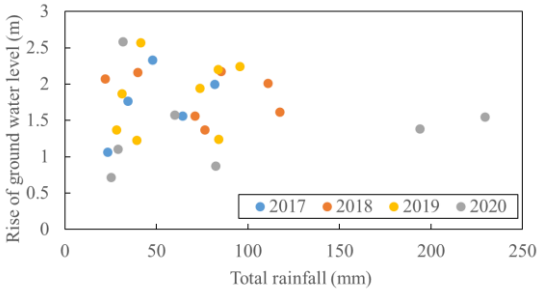

Fig. 10 Relationship between rainfall and water level increase.

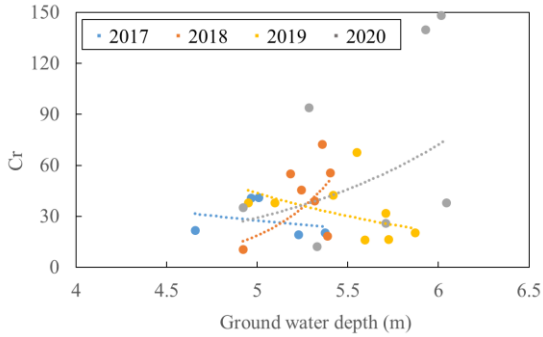

Fig. 11 Relationship between groundwater depth prior to rainfall and rainfall coefficient.

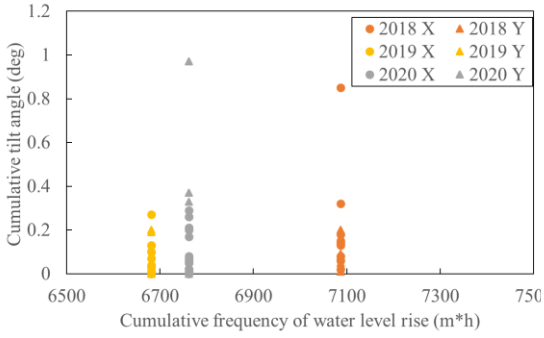

Fig. 12 Relationship between cumulative degree of water level increase and slope angle.

was relatively low.

3. EVALUATION OF SLOPE STABILITY VIA NUMERICAL SIMULATION

The finite difference method (FDM) and finite element method are typical numerical analysis methods that consider the target ground as a continuum. The FDM is more advantageous than the finite element method for performing stress-deformation calculations at each time increment based on explicit formulations because the constitutive laws are easier to formulate [7]–[9]. In this study, we used FLAC [10], which is a large-deformation finite-difference analysis code based on the explicit method developed by Cundall et al. FLAC can be used to perform seepage analysis for porous media independently of stress-deformation analysis. Furthermore, FLAC can be used to perform coupled stress–osmosis flow analyses. A two-dimensional slope model was developed to perform elastoplastic FDM analysis, focusing on the conditions of slope deformation, rainfall, and groundwater depth. Slope stability analyses based on the shear strength reduction method [7] were conducted under different conditions to determine the constituent geological features of the slope. The simulation flow can be categorized into four major aspects: (1) creation of the slope model and setting of physical properties, (2) reproduction of the steady-state of groundwater flow, (3) reproduction of rainfall and groundwater flow, and (4) determination of slope failure via gravity analysis.

3.1 Outline of Slope Model

To reproduce the slope of interest, a numerical model with the same dimensions as those of the slope was created, i.e., 140 m deep and 61.7 m high (Fig. 13). The physical properties used in the analysis were set based on previous studies [11], [12], as listed in Table 1. Figure 14 shows the groundwater depth and rainfall observed in the field, as described in the previous section. It was observed that the groundwater depth on the target slope increased by 1–3 m when the rainfall down the slope was a few tens of millimeters. In addition, the groundwater depth fluctuated immediately after the rainfall, indicating a sensitive response. To reproduce this situation, the following three analyses were conducted: Case 1—analysis of input conditions based on past geotechnical investigations; Case 2—analysis assuming that groundwater flowed more easily in the talus sediment layer around the base surface; Case 3—

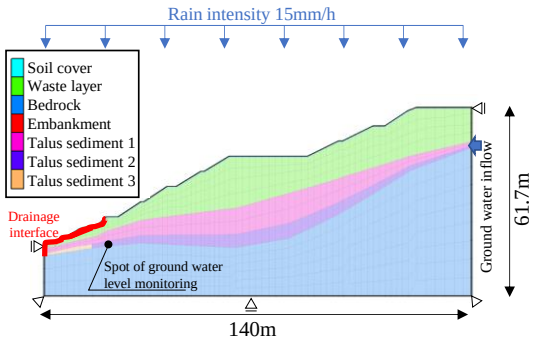

Fig. 13 Cross-section of analysis model.

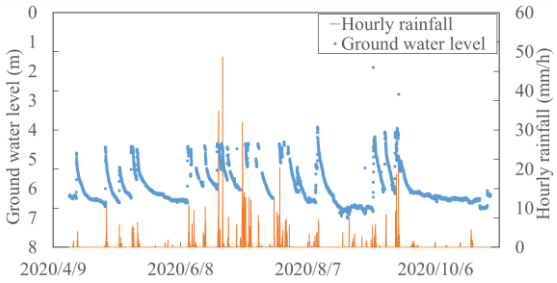

Fig. 14 Observation data of rainfall and groundwater depth.

Table 1 Physical properties.

Layer type	Dry density	Shear resistance angle	Cohiesion	Poisson's ratio	Deformation modulus	Coefficient of permeability		
						Case1	Case2	Case3
	ρ_d (kg/m^3)	ϕ (deg)	c (kN/m^2)	ν(-)	E(MN/m^2)	k (m/s)		
Bedrock	2300	-	-	0.15	1000	5.0×10^{-7}	5.0×10^{-7}	5.0×10^{-7}
Talus sediment 1	1700	35	0	0.3	300	5.0×10^{-5}	5.0×10^{-5}	5.0×10^{-5}
Talus sediment 2	1700	35	0	0.3	300	5.0×10^{-5}	2.5×10^{-2}	2.5×10^{-2}
Talus sediment 3	1700	35	0	0.3	300	5.0×10^{-5}	2.5×10^{-2}	1.0×10^{-2}
Waste layer	1400	37	8	0.3	200	3.0×10^{-5}	3.0×10^{-5}	3.0×10^{-5}
Soil cover	1400	15	10	0.3	200	5.0×10^{-7}	5.0×10^{-7}	5.0×10^{-7}
Embankment	2300	-	-	0.15	300	3.0×10^{-5}	3.0×10^{-5}	3.0×10^{-5}

analysis assuming that the permeability at the end of the slope worsened, in addition to Case 2. The effect of the permeability of the talus sediment layer on the groundwater level increase and safety factors were examined.

3.2 Reproduction of Steady Groundwater Flow and Rainfall

The distribution of groundwater level based on the steady-state of the slope was reproduced. In addition, the validity of reproduction was verified by comparing it with *in situ* data. The groundwater table was reproduced by inflowing groundwater from the higher section of the slope, and the initial saturation of the ground was increased by providing 0.226 mm/h of rainfall from the slope surface. In addition, groundwater corresponding to this amount of rainfall was supplied from the cross-sectional boundary of the talus sediment layer at the higher section of the slope. Figure 15 shows the saturation distribution of the groundwater in the steady-state. In the analysis, the groundwater level in the steady-state was 6.49 m. It was assumed that this value can appropriately reproduce the steady-state water level, even when compared with the lowest water level before rainfall, which was observed at the site as shown in Fig. 14.

3.3 Reproduction of Steady Groundwater Flow and Rainfall

Groundwater flow was applied from the higher side of the slope to simulate a steady surface. Subsequently, a rainfall intensity of 15 mm/h and a total rainfall of 150 mm were applied from the slope surface to reproduce the slope with rainfall. Groundwater inflow from the higher side of the slope increased with rainfall. Figure 16 shows the relationship between rainfall and the groundwater level. A comparison with Fig. 14 shows that the amount of groundwater level increase and the groundwater level both increased immediately after rainfall was reproduced in Cases 2 and 3.

Next, in Cases 2 and 3, the difference in the groundwater level increase was compared when different groundwater inflows Q were imposed from the higher slope. Figures 17 (a) and (b) show the changes in the groundwater level over time for the specified amount of groundwater inflow. These results confirmed that when the amount of groundwater inflow from the higher side of the slope increased, the increased speed of the groundwater level increased as well. In particular, in Case 2, where a water path was assumed in talus

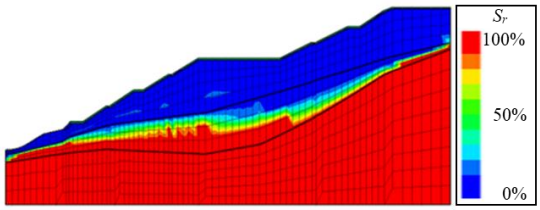

Fig. 15 Saturation distribution in steady state of groundwater.

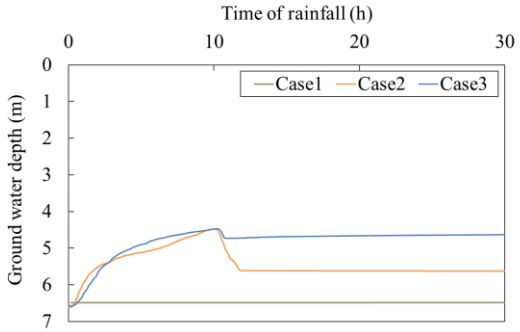

Fig. 16 Relationship between rainfall duration and groundwater depth.

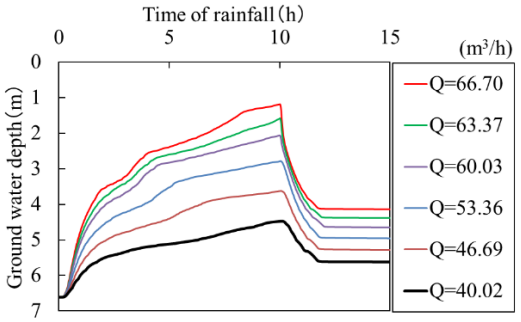

(a) case2

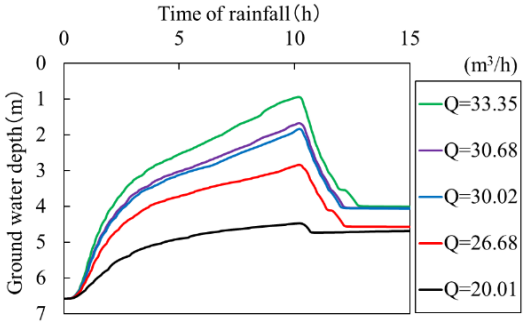

(b) case3

Fig. 17 Relationship between groundwater inflow Q and groundwater level rise.

sediment layers 2 and 3, the inflow that caused the groundwater table to reach a depth of 1 m from the ground surface was approximately 66 m^3/h.

Meanwhile, for the talus sediment layer in Case 3, where it was assumed that the water path was obstructed and the permeability coefficient decreased in material layer 3, it was confirmed that the groundwater level increased at the same level with half the inflow. Hence, the results above clarified that the local obstruction of the water path caused an increase in the pore water pressure in the ground with an insignificant inflow.

3.4 Evaluation of Slope Stability via Gravity Analysis

In this study, the overall safety factor was calculated using the shear-strength reduction method, which is a total stress analysis method that gradually reduces the strength constant of a slope and defines the overall safety factor F_s when the entire slope collapses. The overall safety factor is an index showing the amount of margin that is currently available for the state in which the slope collapses. Generally, it is defined by the following equation based on the magnitude relationship between the sum of the sliding power exerting on the slip soil mass and the sum of the maximum shear resistance on the slip surface:

$$F_s = \frac{\sum R}{\sum S} \quad (1)$$

where ΣR denotes the maximum shear resistance on the slip surface, and ΣS is the sliding power exerting on the slip–soil mass.

When the overall safety factor is less than on1, the slope is defined as collapsed. In addition, the higher the overall safety factor, the greater is the safety of the slope against collapse.

The effect of the increase in the groundwater inflow from the higher side of the slope on the safety factor was confirmed. Figure 18 shows that a slight decrease in hydraulic conductivity at the end of the slope significantly reduced the amount of groundwater inflow required for the safety factor to reduce to below 1.0, which increases the risk of slope failure.

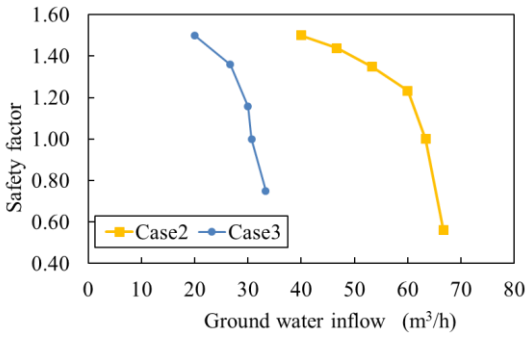

Fig. 18 Relationship between groundwater inflow and slope safety factor.

4. CONCLUSION

In this study, a remote monitoring system was developed using a WSN using the Zigbee communication standard; it was installed and monitored in an outdoor field with a slope. The findings obtained were as follows:

-By measuring the amount of rainfall, groundwater level, and deformation of the ground surface at the site, it was discovered that the change in groundwater level due to rainfall increased by approximately 4 m in a few hours.

-It was confirmed that the tendency of the increase in groundwater level differed every year depending on the rainfall coefficient Cr. It was quantitatively shown that the groundwater flow rate immediately below the slope changed over time.

-In general, an increase in the groundwater level increased the slope deformation. However, monitoring data revealed that the increase in the groundwater level and the amount of deformation on the ground surface were not correlated linearly. It was presumed that this result was primarily due to the abovementioned upward trend of the annual groundwater level change.

In addition, numerical simulations based on monitoring data were performed to calculate the overall safety factor of the slope under different hydraulic conditions of the basement rock. The findings obtained were as follows:

-Based on groundwater level data, a model of the target slope and steady-state groundwater flow was reproduced.

- Water channels were assumed to exist in the talus sediment layer, where it was assumed that the water table was present at all times. Therefore, when a section of this layer was set in the highly permeable region, it was discovered that the water level increased, and the maximum water level immediately after rainfall can be expressed.

Furthermore, assuming that a section of the water path was obstructed, the analysis was performed by setting a low-permeability region. Consequently, it was confirmed that the groundwater level increased to the same extent as the inflow of groundwater based on approximately one-half of the conditions above. Hence, the tendency of the safety factor to decrease was high. In the future, we plan to demonstrate that the risk of slope collapse increases if the permeability below the slope decreases.

5. ACKNOWLEDGMENTS

The authors gratefully appreciate the support provided by Ryota ETO and Naoki YAMADA during their studies. This study was supported by a

research grant from the Japan Construction Information Center Foundation (JACIC). And we would like to thank Editage (www.editage.com) for English language editing.

6. REFERENCES

[1] Nishikawa Y., Sasamura T., Ishizuka Y., Sugimoto S., Iwasaki S., Wang H., Fujishima T., Fujimoto T., Yamashita K., Suzuki T., Kurihara K., Design of stable wireless sensor network for slope monitoring, 2018 IEEE Topical Conference on Wireless Sensors and Sensor Networks, 2018, pp.8-11.

[2] Nishikawa Y., Sasamura T., Ishizuka Y., Sugimoto S., Fujishima T., Fujimoto T., Iwasaki S., Kurihara K., Yamashita K., Problems with independent power supplies in wireless sensor networks, IEICE technical report, Vol. 116, No. 429, EE2016-53, 2017, pp. 27-32. (in Japanese)

[3] Sugimoto S., Sasamura T., Ishida J., Ishizuka Y., Fujishima T., Fujimoto T., Iwasaki S., Yamashita K., Kurihara K., Basic research on the development and application of slope ground measurement systems using wireless sensor networks, Japan Society of Civil Engineers 2016 Annual Meeting, 2016, pp.27-28. (in Japanese)

[4] Ishida C., Sugimoto S., Jiang Y., Omine K., Ishizuka Y., Takaesu R., Iwasaki S., Basic research on the development of multi-point observation method for slope, Western Branch of Japan Society of Civil Engineers 2019 Annual Meeting, 2019, pp.347-348. (in Japanese)

[5] Nakamura T., Sugimoto S., Jiang Y., Omine K., Ishizuka Y., Takaesu R., Iwasaki S., Development of a monitoring system for multi-point observation of slope, Western Branch of Japan Society of Civil Engineers 2020 Annual Meeting, 2020, pp349-350. (in Japanese)

[6] Sugiyama Y., Tsukuda E., Katoh K., Ikeda K., Analyses of groundwater data from observation wells for earthquake prediction in the Tokai District, Japan - An analysis of water level fluctuations (part 1)-, Geological Survey Monthly Report, Vol.32, No.3, 1981, pp.133-150. (in Japanese)

[7] Ishida J., Jiang Y., Omine K., Sugimoto S., Higashi Y., Ogata Y., Numerical study on slope stability in consideration of the influence of weathering by two-phase flow analysis, Proceeding of EUROCK 2015 – ISRM European Regional Symposium – the 64th Geomechanics Colloquy, 2015, pp.997-1002.

[8] Ishida J., Sugimoto S., Jiang Y., Seepage flow behavior in slope model test and verification of reproducibility by numerical simulation, Proceedings of the 8th Asian Joint Symposium on Geotechnical and Geoenvironmental Engineering, 2016, pp.75-80.

[9] Sugimoto S., Jiang Y., Omine K., Ishida J., Higashi Y., Numerical studies on slope stability in torrential rainfall by using two-phase flow analysis, Proceeding of The 15th Asian Regional Conference on Soil Mechanics and Geotechnical Engineering, 2015, JPN-105(6 pages).

[10] Itasca Consulting Group, Inc., FLAC, Fast Lagrangian Analysis of Continua, Theory and Background, 2000.

[11] Chang H., Sugimoto S., Jiang Y., Omine K., Study on stability evaluation of slope ground with rainfall and groundwater flow, 2019, pp.335-336. (in Japanese)

[12] Nakamura M., Sugimoto S., Jiang Y., Omine K., Study on evaluation of mechanical stability of slopes with rainfall and groundwater flow, Western Branch of Japan Society of Civil Engineers 2020 Annual Meeting, 2020, pp.415-416. (in Japanese)